Journal of
Materials Chemistry A

Materials for energy and sustainability

Accepted Manuscript

This article can be cited before page numbers have been issued, to do this please use: Y. S. Ye, M. G. Mohamed, C. W. Chen and S. Kuo, *J. Mater. Chem. A*, 2023, DOI: 10.1039/D2TA09232H.

ROYAL SOCIETY OF CHEMISTRY

rsc.li/materials-a

View Article Online
DOI: 10.1039/D2TA09232H

Journal Name

ARTICLE

Integrating the multi-functionalities in metalloporphyrin porous organic polymers enabling strong polysulfide anchors and rapid electrochemical kinetics in Li-S battery

Received 00th January 20xx,
Accepted 00th January 20xx

DOI: 10.1039/x0xx00000x

www.rsc.org/

Yun Sheng Ye*, Mohamed Gamal Mohamed, Cheng Wei Chen, and Shiao Wei Kuo*

Ready lithium polysulfide (LiPS) diffusion and sluggish redox kinetics hamper lithium-sulfur (Li-S) batteries toward high cyclability and rate capability. Herein, metalloporphyrin-based porous organic polymers [Por(M)-POPs] integrated with electrolyte accessible, Li-ions conductive, LiPS-trapped, and LiPS-catalytic functions were elaborately engineered by constructing a conformal Por(M) and imidazolium connector to form the 2D polymeric ionic liquid (PIL) framework through click reaction. The synthesized POPs are incorporated with a single-atomic catalyst and fully exposed lithiophilic sites to afford effective catalysis and robust chemical/physical barrier for LiPSs as well as improve electrolyte affinity and Li-ion transport. Consequently, the coordinated Mg or Co atoms Por(M)-POP hybridized with graphene nanosheet (GN) as separator coatings, our Por(M)-POP/GN-modified separators showed a high initial capacity of >1500 mAh g^{-1} at 0.1 C, stable cycling life (only <0.05% capacity decay rate per cycle at 1 C) with 1000 cycles, excellent rate performance (>830 mAh g^{-1} at 2 C), anti-self-discharge ability, and high areal capacity up to 2.8~3.1 mAh cm^{-2} with a sulfur loading of ≈4 mg cm^{-2} after 100 cycles. This work opens up a new insight into POP integrating single-atomic catalysts and PIL framework to effectively alleviate LiPS shuttling and accelerate electrochemical kinetics.

Keywords: metalloporphyrin, polymeric ionic liquid framework, porous organic polymer, electrocatalysis, lithium polysulfide, lithium-sulfur battery

Introduction

The ever-growing demand for clean and renewable energy in portable electronic devices, long-range electric vehicles (EVs), and grid-scale energy storage systems (ESSs) urgently calls for advanced rechargeable batteries with high energy density, long-term cycling stability, and low cost.[1,2] Lithium-sulfur (Li-S) batteries are considered ideal candidates for energy storage devices due to their high theoretical energy density (2600 Wh kg^{-1}) and capacity (1675 mAh g^{-1}).[3] Also, the active sulfur as cathode material shows prominent advantages in earth-abundance, environmental friendliness, and cut price.[4] However, the practical application of Li-S batteries is severely hindered by the rapid capacity degradation, low Coulombic efficiency, and cycling instability due to poor electronic conductivity of sulfur and dissolution of soluble intermediate lithium polysulfides (LiPSs, Li_2S_x, $4 \le x \le 8$) between cathode and anode described as the "shuttle effect".[5,6] More importantly, the solid-solid conversion reaction of $Li_2S_2 \rightarrow Li_2S$ (50% theoretical capacity), regarded as the rate-controlling step, is very sluggish because of its nonconductive nature and high activation energy, resulting in premature termination of the discharge and low utilization of sulfur active material.[7,8] Therefore, most of the current research on Li-S batteries has extensively concentrated on the shuttle effect of soluble LiPSs and $Li_2S_4 \rightarrow Li_2S$ conversion reactions, which are decisive in acquiring a high theoretical capacity.

Until now, various strategies through rational engineering of separators have addressed the problem of the LiPSs' shuttling to a certain extent by modifying electrically conductive carbonaceous materials with functionalized groups to accelerate electron transport and physical trap/chemical trapping for dissolved LiPSs.[3,9-11] However, the enhancement in electronic properties of sulfur species and alleviation in the diffusion of LiPSs is not enough to achieve an advanced Li-S battery due to the high activation energy of solid-solid conversion. Fortunately, an accelerating effect for the sluggish conversion of LiPSs from the liquid to solid state in Li-S batteries can be achieved by introducing specific modifiers with catalyst effects on the separators facing the S-cathode. For example, indium nitride (InN) nanowires as LiPS catalyzers were introduced into modified separators by mixing with Super P and polyvinylidene fluoride (PVDF) binder, showing mitigated shuttling and accelerated conversion for LiPSs.[12] Single Ni atoms

[a] *Department of Materials and Optoelectronic Science, National Sun Yat-sen University, Kaohsiung, 80424, Taiwan*
E-mail: ysye@mail.nsysu.edu.tw; kuosw@faculty.nsysu.edu.tw.
Electronic Supplementary Information (ESI) available: [details of any supplementary information available should be included here]. See DOI: 10.1039/x0xx00000x

View Article Online
DOI: 10.1039/D2TA09230H

on nitrogen-doped graphene (Ni@NG) as separators' modifiers enable trapping the LiPSs and accelerating the kinetic transformation of LiPSs.[13] Besides, polyaniline (PANI) encapsulated amorphous vanadium pentoxide (V_2O_5) nanowires (VOH@PANI) were synthesized and utilized as a fundamental building block for the preparation of modified separator, showing enhanced properties of LiPS adsorption, catalytic activity, and ionic conductivity.[14] Among catalytic materials, single atomic catalysts (SACs) integrated merits of homogeneous and heterogeneous catalysts provide well-dispersed and efficient atomic-level catalytic sites, which can catalyze the mutual conversion between liquid and solid LiPSs, thereby effectively accelerating the reaction kinetics and reducing the polarization of Li-S batteries.[15-17]

Porphyrin (Por) architectures containing four pyrrolic nitrogen sites could readily incorporate and stabilize various metal ions to form metalloporphyrins, which could serve as light harvesters, oxygen carriers, and catalysts.[18,19] When employing metalloporphyrin [Por(M)] as an electrocatalyst in working Li-S batteries, the characteristics of the sulfur redox reactions were tailored, performing enhanced redox kinetics and a regulated phase transition mode.[20,21] Incorporating Por(M) architectures into porous organic polymers (POPs) to form M-N_x active sites has been proven effective in developing SACs in Li-S batteries. More recently, some Por(M)-based POPs [Por(M)-POPs] combined with carbonaceous materials have been reported as efficient catalytic modifiers for the separator or electrode to achieve high-performance Li-S batteries.[22-25] However, the inhibitory and affinity functionalities of these POPs on the LiPS shuttling and the electrolyte are limited, respectively. Therefore, it is very challenging to integrate strong LiPS-anchor ability through physical trap and chemisorption, as well as easy electrolyte accessibility and rapid Li-ion diffusion in electrically catalytic Por(M), rendering remarkable performance improvement in Li-S batteries.

In this contribution, a multi-function integrated Por(M)-based material is rationally designed to mitigate the LiPS shuttling and promote the kinetics of the multiphase sulfur redox reactions by enhancing Li-ion accessibility and electrocatalysis effect in working Li-S batteries. Specifically, Por(M), coordinated with Mg or Co [denoted as Por(Mg/or Co)], electrocatalytic active sites are constructed *via* covalently bonded by polymeric ionic liquid (PIL) network with the imidazolium cations and bis(trifluoromethane)-sulfonimide ($TFSI^-$) anions to form POP, as illustrated in **Scheme 1**. Among the coordinated metals, Mg and Co atoms are two of the most important naturally occurring metalloporphyrins found in chlorophylls and vitamin B12, respectively.[26] The formed imidazolium-containing connectors endow the POP with LiPS trapping, electrolyte affinity, and ionic dissociation functions originating from their high intrinsic polarity, polarizability, and ion conduction. On the one hand, the ion-conductive linkers integrate the Por(M) active sites within the porous structure for easy accessibility of liquid electrolytes and effectively decoupled charge transport in electrolytes. On the other hand, the connector consisting of imidazolium cations shows a good affinity for the electrically conductive graphene nanosheet (GN) *via* strong cation-π interactions,[27] which facilitate the formation of Por(M)-POPs/GN nanohybrids and allow fast electron transport. The as-designed nanohybrids assisted by polymeric binder were modified on a commercialized Celgard separator by a simple blade-coating for high-performance Li-S batteries. The Por(M)-POP modifiers provide rich chemisorption sites and porous structures for chemically/physically trapping the LiPSs as well as a high affinity for rapid electrolyte infiltration and ion diffusion. Notably, the Por(M)-POP in the constructed 3D continuous ion/electron conductive nanohybrid exerts extraordinary catalysis effect in LiPS conversion reaction, showing larger specific capacity, higher rate performance, and enhanced cycle stability.

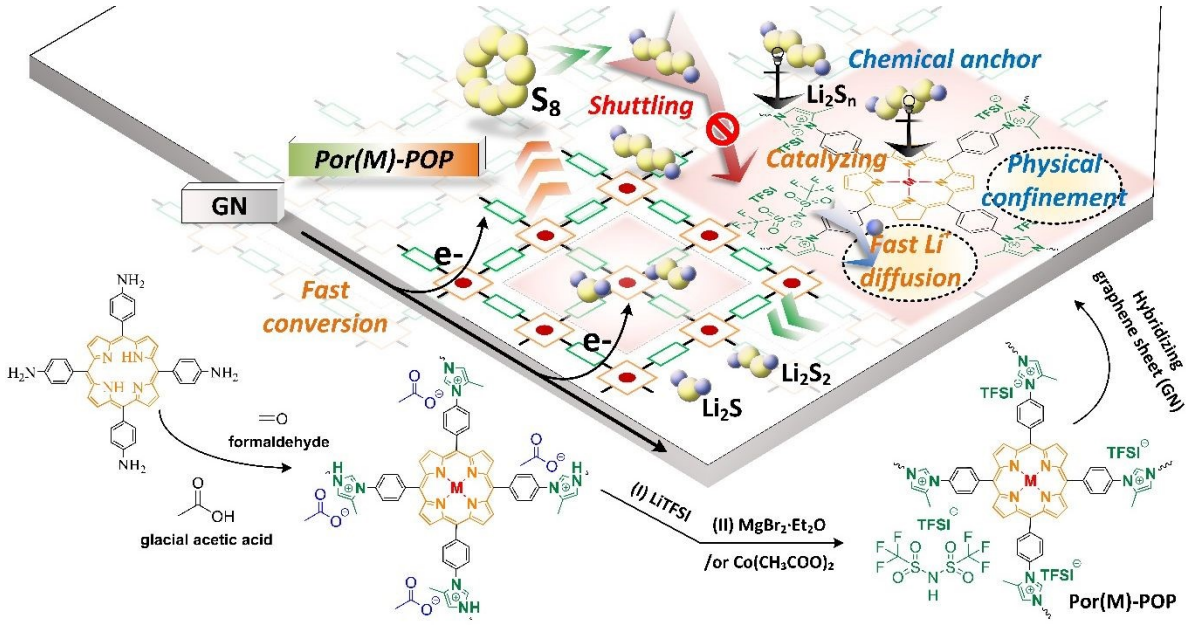

Scheme 1. Schematic illustration of the synthesis for the Por(M)-POP/GN modified separators and its efficient inhibition and catalyst for LiPS in the electrochemical process.

View Article Online
DOI: 10.1039/D2TA09232H

Journal Name

ARTICLE

Experimental

Preparation of the Mg/or Co coordinated porphyrin-based porous organic polymers [Por(Mg)-POP and Por(Co)-POP]

***Synthesis of meso-(4-nitrophenyl) porphyrin (TNPP)*:** 5.5 g (36 mmol) 4-nitrobenzaldehyde and 6 mL (63 mmol) acetic anhydride were added in a 250 mL flask with steering at 120 °C. Then, the mixture of 2.5 mL (36 mmol) pyrrole and 10 mL propanoic acid was slowly added to the flask and reacted for another 1 h. Followed by cooling to room temperature, filtrating, washing with methyl alcohol until the filtrate becomes colorless, and vacuum drying at 60 °C to get coarse TNPP with atropurpureus color. Next, the coarse TNPP was extracted by Soxhlet extractor with acetone until the color of extracting solution from deep purple to pale yellow. Finally, recrystallized by pyridine to get TNPP with light purple color. The yield is ≈67%.

***Synthesis of meso-(4-aminophenyl) porphyrin (TAPP)*:** 3.1 g (≈3.9 mmol) TNPP and 150 mL HCl were added in a 250 mL flask with steering at room temperature for 0.5 h. Next, the solution of 8.9 g (39 mmol) $SnCl_2{\cdot}2H_2O$ in 30 mL HCl was added and reacted at room temperature for 2.5 h and then increased to 70 °C for 7 h with N_2. Followed by cooling to room temperature, filtrating, solvating the filter residue in 500 mL distilled water, adjusting pH to 8 with deep purple color, filtrating, washing with water until the filtrate became colorless, washing with methyl alcohol and vacuum drying at 60 °C to get coarse TAPP. Finally, the coarse TAPP was purified by column chromatography with neutral alumina as the stationary phase and CH_2Cl_2/CH_3OH (V: V = 12:1) mixture as eluent. The yield is about 84%. ^{1}H NMR (400 MHz, DMSO-d_6, δ ppm) 8.90 (s, 8H), 7.87 (d, *J*=8.2 Hz, 8H), 7.02 (d, *J*=8.2 Hz, 8H), 5.59 (s, 8H), -2.71 (s, 2H). ^{13}C NMR (400 MHz, DMSO-d_6, δ ppm): 149.17, 141.34, 136.83, 134.27, 128.03, 126.98, 123.95, 120.32, 115.04.

***Synthesis of Por(Mg/or Co)-POPs*:** 0.44 g (0.65 mmol) TAPP, 8 mL glacial acetic acid, and 8 mL water were added to a 50 mL flask at room temperature. Next, 0.39 mL (5.3 mmol) 37% formaldehyde solution, 0.81 mL (5.3 mmol) 40% pyruvaldehyde solution, 2 mL glacial acetic acid, and 2 mL water were added and reacted at room temperature for 0.5 h and then increased to 80 °C for 12 h. Followed by cooling to room temperature, filtrating, washing with DI water until the filtrate becomes colorless, and extracting with CH_3OH for 24 h to get crude Por-POP with acetate anions (OAc^-). The resultant was further treated with LiTFSI in an aqueous solution for 24 h, filtrating, washing with DI water, and vacuum drying at 60 °C to obtain Por-POPs. Por(Mg)-POP [Por(Co)-POP] was obtained by coordination reaction with 0.58 g (≈0.62 mmol, theoretical structural unit) Por-POP, 4.80 g (19 mmol) $MgBr_2{\cdot}Et_2O$ [5.42 g (19 mmol) of $Co(CH_3COO)_2$], and 50 mL DMF reflux steering for 12 h at 150 °C (120 °C) with N_2, filtrating, washing with DI water, and vacuum drying at 60 °C.

Preparation of Por-POP/GN, Por(Mg)-POP/GN, and Por(Co)-POP/GN nanohybrid functionalized separators

The Por-POP/GN, Por(Mg)-POP/GN, and Por(Co)-POP/GN nanohybrids were firstly prepared by mixing 15 mg Por-based POPs with/without coordinated metals and 5 mg GN in anhydrous NMP and sonicating for 1 h at room temperature, leading to uniform nanohybrid suspensions. The resulting nanohybrid suspension was mixed with 5 mg polyvinylidene difluoride (PVDF) and cast onto Celgard, followed by solvent evaporation at 60 °C under vacuum for 24 h. The obtained modified separators are denoted as Por-POP/GN, Por(Mg)-POP/GN, and Por(Co)-POP/GN with mass loading of ≈0.25 mg cm^{-2} for the regular tests. The content of Mg and Co atoms in the coating layer determined by X-ray photoelectron spectroscopy (XPS) were 3.8 and 4.4 wt%, respectively.

Results and discussion

The stepwise preparation of the Por(M)-POP was schematically illustrated in **Scheme 1**. Using the Debus-Radziszewski "*click*" reaction, the TAPP monomers were covalently bonded to synthesize Por-POP and then ion-exchanged by LiTFSI salt to tune imidazolium connector from hydrophilic OAc^- to hydrophobic $TFSI^-$ anions. The successful synthesis of Por-POP was verified by analyzing its characteristic Fourier transform infrared (FTIR) spectra and solid-state ^{13}C NMR spectroscopy. FTIR of TAPP in **Figure 1a** shows the peak at 3352 cm^{-1} corresponding to the N-H stretching vibration of amino groups became broader, and the peak at 1615 cm^{-1} corresponding to the stretching vibration of the benzene ring shifted to a lower wavenumber of 1601 cm^{-1} after the click reaction. Moreover, the synthesized POPs maintain the characteristic peak corresponding to the C-N stretching vibration of pyrrole at 1471 cm^{-1} and produce new peaks corresponding to the CF_3 and SO_2 of $TFSI^-$ anions at 1227 and 1347 cm^{-1}, respectively, verifying successful reaction and anion exchange. After the metalation of Mg or Co ions, the stretching and bending of the N-H bond related to free base Por at 960 cm^{-1} disappeared, and the functional groups of Mg-N or Co–N bonds were established at 997 cm^{-1}, which resulted in forming Por(M) complex in POPs. ^{13}C NMR of Por-POP in **Figure S1** also shows the characteristic peaks related to aromatic carbons and Por in region 120-160 ppm. For morphological analyses, both Por(M)-POPs show the disordered laminar structure with large

View Article Online
DOI: 10.1039/D2TA09273H

nanoscaled pores in the transmission electron microscopy (TEM) images (**Figure 1b**). Besides, their X-ray diffraction (XRD) characterization in **Figure S2** presenting an amorphous structure is similar to the as-prepared Por-POP. By Brunauer-Emmett-Teller (BET) surface area analysis (**Figure S3**), the Por(M)-POPs show type-IV isotherms with type H3 hysteresis loops, indicating the synthesized POP containing both micro and meso pores. The specific surface area of Por(Mg)-POP and Por(Co)-POP was determined to be 275 and 283 $m^2 g^{-1}$, which could provide more active sites and 3D diffusion channels to achieve effective physical/chemical LiPS adsorption and fast Li-ion conduction, respectively.

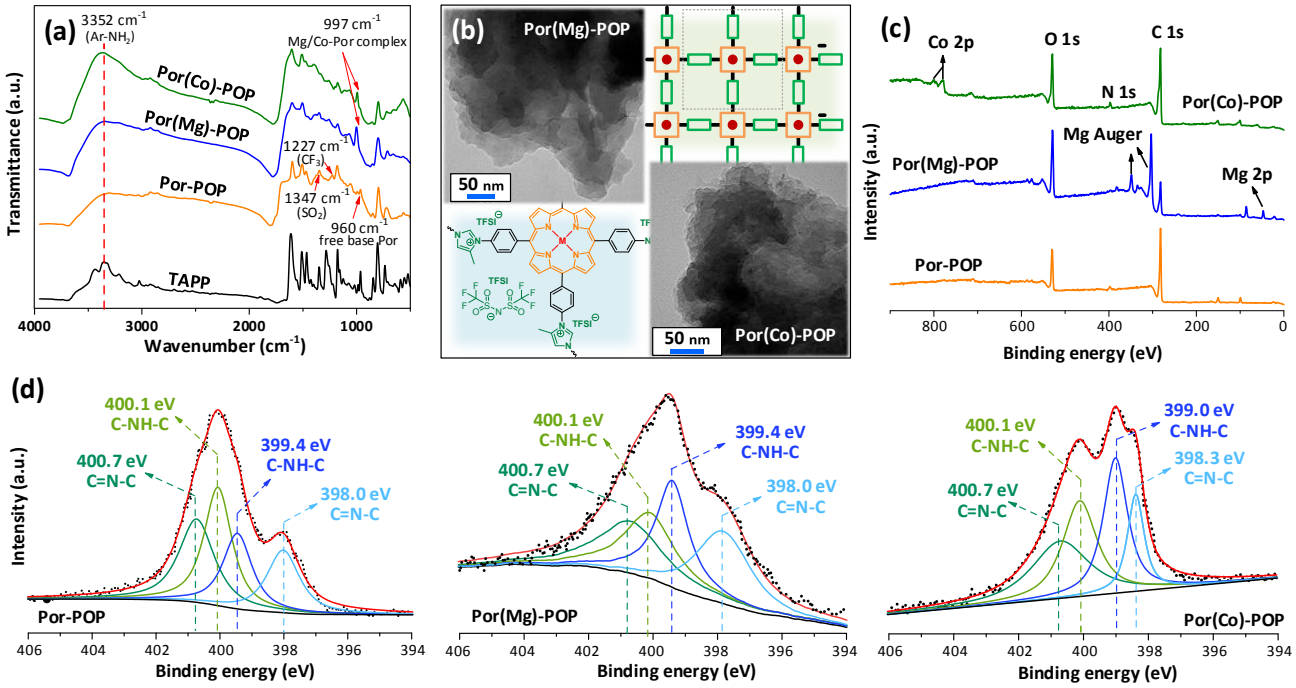

Figure 1. (a) FTIR of Por-POP and Por(Mg)-POP and Por(Co)-POP; (b) TEM of Por(Mg)-POP and Por(Co)-POP; XPS of Por-POP, Por(Mg)-POP and Por(Co)-POP: (c) wide range and (d) N 1s spectra.

As shown in **Figure 1c**, the XPS scan spectra clearly display C 1s, N 1s, and O 1s peaks for all POPs with and without metal coordination and apparent signals assigned to Mg auger (304.1 and 349.5 eV) and Co 2P (779.1 and 794.9 eV) for Por(Mg)-POP and Por(Co)-POP, respectively.[28,29] And the mass contents of Mg and Co atoms in weight percentage of the prepared Por(Mg)-POP and Por(Co)-POP were determined to be 5.0 and 5.8 wt%, respectively. In addition, the high-resolution N 1s spectra of Por-POP can be resolved into four signals with binding energies of 398.0 (C=N-C) and 399.4 (C-NH-C) eV for pyrrolic-N as well as 400.1 (C-NH-C) and 400.7 (C=N-C) eV for imidazolium-N (**Figure 1d**).[30,31] Due to the slight difference between the binding energies of M-N and pyridinic-N, the signal of coordinated metal Por-ring is incorporated into the peak at ≈398.0 eV.[32,33] Those results confirmed the successful metallization of Por-POP with Mg or Co. SEM and corresponding EDS mapping in the material of both Por(Mg)-POP and Por(Co)-POP have been carefully analyzed and shown in **Figure S4a-S4h**. The result offers EDX elemental maps of C, O, Mg, and Co to identify the distribution of the different elements within representative Por(M)-POPs. Both Por(M)-POPs present an even distribution of C, O (corresponding to the oxygen of TFSI ions), and metal atoms [Mg and Co for Por(Mg)-POP and Por(Co)-POP, respectively]. Moreover, both Por(M)-POPs displayed a uniform and high-density single-atom dispersion, as shown in the TEM of **Figures S4i** and **S4j**. Moreover, the thermal decomposition temperatures corresponding to 5 % weight loss ($T_{d5\%}$) of all POPs are >230 °C (**Figure S5**), demonstrating the good thermal stability for Li-S batteries.

The chemisorption capacity for LiPSs was explored in the visualized vials, as shown in **Figure 2a** (inserted picture); the same amount of both Por(M)-POPs was added to the same concentration of Li_2S_6 solution (~0.09 M) for 24 h. The brown Li_2S_6 solution did not become light but got darker due to a small amount of dark Por(M)-POPs dispersed in the solution.[34] Therefore, the concentration of residual Li_2S_6 solution in the resulting supernatants was further examined by ultraviolet-visible (UV-vis) absorption spectroscopy. As shown in **Figure 2a**, the intensity of the characteristic peak (S_6^{2-}) at ≈280 nm declines sharply after adding Por(M)-POPs in the Li_2S_6 solution. For the substratum precipitated powder, the N 1s XPS spectrum was applied to test the interaction force between the Por(M)-POP and Li_2S_6. In **Figure 2b**, the characteristic peaks of pyrrolic-N and imidazolium-N exhibit a positive shift after adsorbing Li_2S_6, implying charge transfer from electron-rich N atoms by both Por-ring and imidazolium connector to Li ions. Moreover, new peaks emerged at 402~405 eV, manifesting a strong affinity to Li through chemical interaction.[35] To further confirm the interaction between LiPSs and the S-metal center of Por(M)-POP, the high-resolution Mg 2p (**Figure S6**) and Co 2p (**Figure**

View Article Online
DOI: 10.1039/D2TA09232H

2c) spectra before and after adsorbing Li_2S_6 solution were examined. From the XPS spectra, the Mg 2p spectrum of Por(Mg)-POP shows a negative shift of ≈0.7 eV.[36] The Co 2p spectrum shows two pairs of spin-orbit doublets, Co $2p_{3/2}$ (782.3 eV) and Co $2p_{1/2}$ (798.3 eV), and two broad satellite peaks in the Por(Co)-POP. Due to the Lewis-base interaction between unsaturated Co and S atoms, the binding energy of entire Co spectra reveals a negative shift of ≈0.5 eV after the adsorption of Li_2S_6 [Por(Co)-POP/Li_2S_6].[37] These observations indicated the simultaneous interactions between Li-N rich skeleton and the S-metal center are beneficial for effective inhibition in the LiPS shuttling. The physical trap capacity of the synthesized Por(M)-POPs for LiPSs was measured in matryoshka visualization devices.[38] As shown in **Figure S7**, the small bottle containing brown Li_2S_6 solution with the separator seal was inserted in the giant bottle containing blank electrolyte. The brown Li_2S_6 in small bottles can diffuse into big bottles because of the concentration gradient. The transparent electrolyte in the big bottle with the pristine Celgard (commercial separator) became faint yellow within only 2 h, while the other with POP-modified separators was still colorless. After standing for 24h, the color in both bottles with the Celgard was unchanged due to rapid LiPS penetration through the porous Celgard. By contrast, the color in big bottles with all POP-modified separators is much lighter than the small bottles even after one week of storing, meaning physical barriers were consistently effective in mitigating LiPS shuttling.[6]

Strong interaction between the Por(M)-POP and Li_2S_6 may avail the charge transfer conductive matrix to adsorb LiPSs and corresponding LiPS redox.[39] The symmetric cells were assembled by sandwiching 0.2 M Li_2S_6 electrolyte (DOL/DME, V/V=1:1) contained between two identical working and counter electrodes to investigate the redox kinetics of LiPS. Cyclic voltammetry (CV) test of the symmetric cells using GN, Por(M)-POP/GN hybrids as identical electrodes were conducted within a voltage window of -0.8 to 0.8 V *vs.* Li/Li^+ at 2 V s^{-1}. The symmetric cell with GN in **Figure 2d** shows the polarization curves, mainly attributing to the redox current of Li_2S_6 rather than the capacitive current, as testified by the Li_2S_6 free symmetrical cell.[40] The symmetric cells with Por(M)-POP/GN electrodes display a much higher polarization current intensity and more defined redox peaks than GN, implying a practical catalytic effect for sulfur species conversion due to the existence of Por(M) structures. In addition, the electrochemical impedance (EIS) of the symmetric cells shows a smaller semicircle for the Por(M)-POP/GN compared to GN, indicating faster redox kinetics and efficient charge transfer after the introduction of the Por(M)-POP (**Figure 2e**).[41]

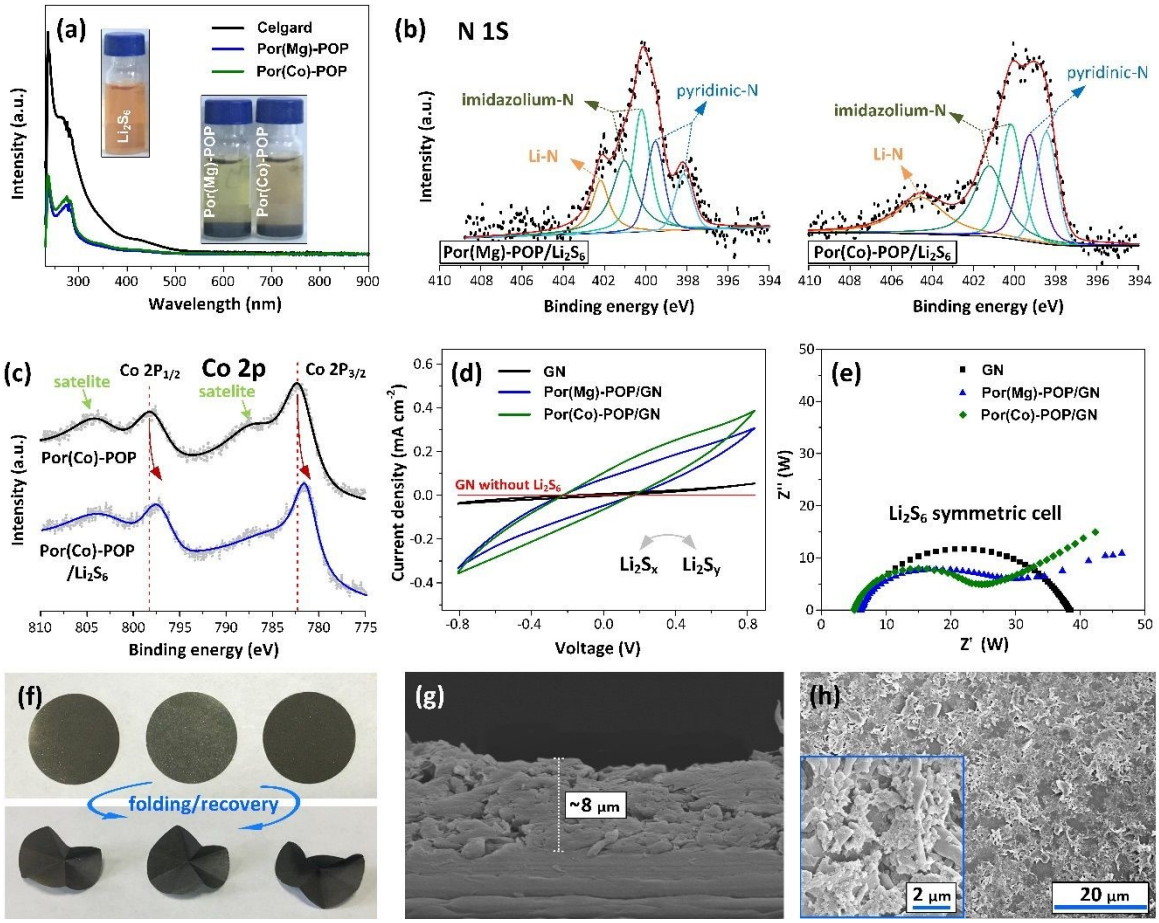

Figure 2. (a) Digital images (insert) and UV-vis adsorption spectroscopy of the original Li_2S_6 solution and the solution with 24 h static adsorbed by Por(M)-POPs; XPS (b) N 1s and (c) Co 2p spectra of Por(M)-POPs; (d) CV curves and (e) EIS spectra of cathodes symmetric cells employing GN and Por(M)-POP/GN as identical electrodes at 2 V s^{-1}; (f) folding/recovery test of Por-POP/GN and Por(M)-POP/GN functional separators; SEM images of (g) cross section and (h) surface of Por-POP/GN modified separator.

View Article Online
DOI: 10.1039/D2TA09232H

Journal Name

ARTICLE

Based on the above results, both Por(M)-POPs have strong LiPS-anchor ability and improved electrochemical kinetics for sulfur species conversion, which are superior candidates for enhancing Li-S battery performance. A facial slurry coating method was employed to modify the commercial Celgard with POP/GN hybrids [noted as Por-POP/GN, Por(Mg)-POP/GN, and Por(Co)-POP/GN], and the coating side was faced to S-cathode.[6] After coating the hybrids, the Celgard was evenly covered by dark skin in the optical photographs [**Figure 2f**, Por-POP/GN, Por(Mg)-POP/GN, and Por(Co)-POP/GN modified separators from the left to the right side]. After the folding and recovery, no modifier peel-off from the Celgard substrate indicates good adhesion between the modifier and the substrate. Furtherly, cross-section scanning electron microscopy (SEM) images of the Celgard and the modified separators are displayed in **Figures 2g**, **2h,** and **S6**. The thickness of the modified layer was well-tunned to ≈8 μm (**Figure 2g**), corresponding to a mass loading of ≈0.25 mg cm^{-2}, which was determined by the cross-section image of the modified separator (Por-POP/GN modified separator as an example). Compared to the large pores with several-hundred nanometres where the dissolved LiPSs can easily pass through for the Celgard, the pores are well covered for the modified separators. As displayed in **Figure S8**, the electrolyte droplets immediately spread on the modified separators (contact angles ≤15°), whereas the droplet located on the Celgard with a larger contact angle (≈41°). The electrolyte uptakes (*EU*) and retentions (*ER*) are measured by soaking separators in electrolytes and then depositing them in an oven at 30 °C, respectively. As shown in **Table S1**, the modified separators offer a much higher *EU* of >172% compared to 70.8% for the pristine Celgard. In addition, the *ER* at different deposition times of the modified separators is higher than the Celgard. The result indicates that the modifier consisting of imidazolium connectors and the porous structure is conducive to enhancing the compatibility of the separator/electrodes interface and the diffusion of Li-ions through the separator.

The electrochemical stability window of different separators was researched by linear sweep voltammetry (LSV) curves from 0 to 5.5 V with a scan rate of 10.0 mV s^{-1}. The oxidation current related to the Celgard in **Figure S9** is still up to 4.6 V after modifying the POPs, implying the commendable electrochemical stability of the modifiers. **Figure 3a** displays the electrochemical impedance spectroscopy (EIS) plots of stainless steel (SS)|separator|SS symmetrical cells. The measured ionic conductivity is 0.27 mS cm^{-1} for the Celgard, which is increased to 0.62 mS cm^{-1} for all modified separators. The enhanced ionic conductivity may benefit from the synergistic contributions of the improved affinity and uptake for the electrolyte. Next, the separator's Li-ions diffusion coefficient (D_{Li^+}) was calculated by a series of CV with various rates from 0.2 to 0.5 mV s^{-1}. In CV profiles, the cathodic peaks at 1.8-2.1 V and 2.2-2.4 V are assigned as peaks A and B, representing two-step reduction of sulfur, including the insoluble Li_2S_2/Li_2S at low voltage and soluble LiPSs at high voltage, respectively, while the anodic peak corresponding oxidation at 2.3-2.5 V is noted as peak C.[42] The cells with the modified separators show much better curves than those with the Celgard (**Figure S10**), indicating better electrochemical cyclic stability. Further, the first cell cycle with the modified separators is singled out in **Figure 3b**. The modified separator assembled cells reveal a smaller voltage gap (ΔV) between the oxidation and reduction peaks than the cell with Celgard, demonstrating the least polarization and fastest electrochemical redox kinetics.[43] In addition, the cells with modified separators revealed sharper current peaks (**Figure 3c**) than those of Celgard, particularly for the Por(Co)-POP/GN functional separator, indicating higher electrochemical reversibility and more facile LiPS conversions.[44] The classical Randles-Sevick equation was used to quantitatively calculate the D_{Li^+}, which is based on the slope of the linear plot of the peak current (I_p) versus the square root of the scan rate ($V^{0.5}$) (**Figure S11**).[45] As shown in **Figure 3d** and **Table S2**, the D_{Li^+} value was significantly improved by introducing functional POP-based modifiers. Although the improvement was slightly slowed down by replacing metalloporphyrin; however, their connector containing the lithiophilic imidazolium group facilitated Li-ions diffusion.[6,35]

View Article Online
DOI: 10.1039/D2TA09232H

Journal Name

ARTICLE

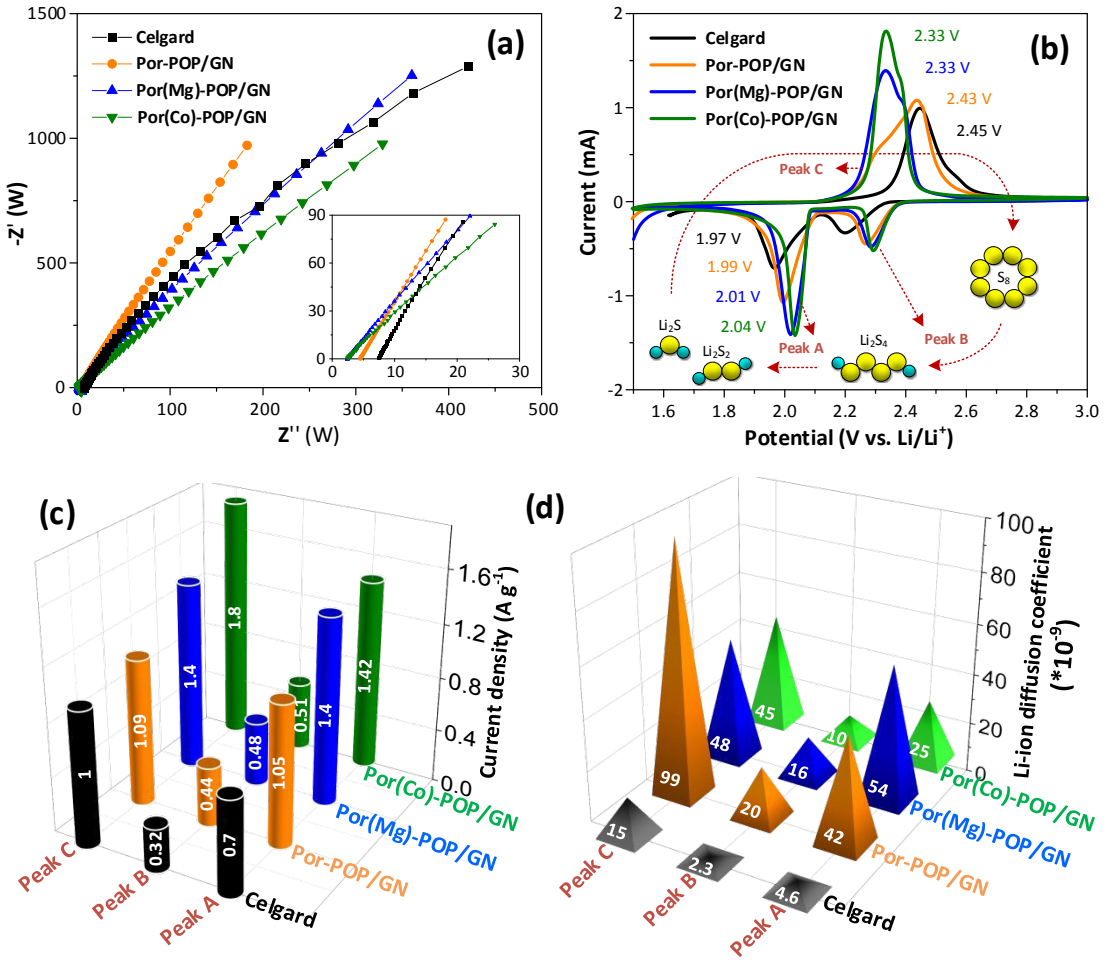

Figure 3. (a) EIS plots of the different separators; (b) CV curves of the cells with various separators at a scan rate of 0.2 mV s^{-1}; (c) peak currents and (d) Li-ion diffusion coefficient of the cells with various separators.

The long-term cycling performance of cells with various separators was measured at 1 C for 1000 cycles. **Figure 4a** displays the galvanostatic charge-discharge profiles of the cells with various separators at a current of 1 C for the 5th cycle. Similar to the CV observation, there are two distinct voltage platforms at ≈2.3 and ≈2.1 V, corresponding to S_8→Li_2S_4 and Li_2S_4→Li_2S_2/Li_2S, contributing to 25% and 75% of theoretical capacity in Li-S batteries. The profile showed that the cell with modified separators had more negligible polarization (ΔV=0.24~0.28 V, determined by 50% of specific capacity) and a more extended and smoother voltage platform than those of the Celgard assembled cell (ΔV=0.37 V). As displayed in **Figure 4b**, the cell with the Celgard suffers from a quick drop in specific capacity due to the profound "shuttle effect" of LiPSs during the fast charge-discharge cycles. In contrast, the Por-POP/GN modifier can effectively chemically/physically anchor LiPSs so that more sulfur species can be constrained, leading to a higher specific capacity and cycling stability. Impressively, the Por(M)-POP/GN modified separators exhibit a high initial specific capacity but an adequate capacity of >600 mAh g^{-1} after 1000 cycles. The capacity fading rate of the cells also showed lower values of 0.052% and 0.046% specific capacity loss per cycle for Por(Mg)-POP/GN and Por(Co)-POP/GN, respectively, than that of Celgard (0.174%) and Por-POP/GN (0.075%), attributing to the synergistic effect of metalloporphyrin center and imidazolium connector for expediting the solid-solid conversion.

To further investigate the cells' upper-plateau discharge specific capacity (Q_H) and lower-plateau discharge specific

capacity (Q_L), the LiPSs-anchor ability and redox reaction availability of the separator can be quantitatively evaluated, respectively.[46] As shown in **Figures 4c** and **4d** show that the cells with modified separators possess higher Q_H and Q_L values than the Celgard assembled cell. Notably, after 905 cycles, the Por(Mg)-POP/GN and Por(Co)-POP/GN modified separators still show higher Q_H and Q_L values, *i.e.,* 237 and 368.5 mA h g^{-1} corresponding to 56.6% utilization and 29.3% retention, 245 and 424.7 mAh g^{-1} corresponding to 58.5% utilization and 33.8% retention, respectively, than the Por-POP/GN modified separator (Q_H utilization: 32.0%, Q_L retention: 15.5%), demonstrating that the metallization of metal ions significantly improve redox reaction kinetics in both conversions of elemental sulfur to soluble LiPSs and growth of Li_2S_2/Li_2S. Besides, they still preserved the two discharge plateaus after 305 cycles (**Figure 4f-4h**), whereas only one discharge plateau was retained after 305 cycles for the Celgard assembled cell (**Figure 4e**) due to the severe polarization.

The rate performance of cells with various separators was examined at stepwise current rates from 0.1 to 2 C, as displayed in **Figure 5a**. The cells with modified separators delivered a much higher initial specific capacity of >1500 mA h g^{-1} than the Celgard-assembled cell (1038 mA h g^{-1}) at 0.1 C. With the increasing current density, the Celgard assembled cell's specific capacity reduced sharply; only 191 mA h g^{-1} can be obtained at 2 C, corresponding to an 18.4% retention rate compared with the initial value. In contrast, a much higher specific capacity retention rate of 51.1% can be maintained for the cells with Por-POP/GN, especially for employing Por(M)-POP/GN as modifiers (>55%). Moreover, the Por(M)-POP/GN assembled cells reversibly recovered their specific capacity to an adequate value and kept a higher utilization ratio at various rates (**Figure 5b**), suggesting excellent reversible stability. **Figure S12** shows cells' corresponding typical charge-discharge profiles with different separators at multiple rates ranging from 0.1 to 2 C. The discharge voltage plateau of the Celgard severely shrunk at a high current density of 2 C due to the sluggish redox reaction. After replacing the Celgard with modified separators, two stable and flat discharge plateaus can be well retained, especially for Por(M)-POP/GN modified separators. Besides, the ΔV between charge and discharge plateaus at various rates display that the cells with Por(M)-POP/GN modified separators have more negligible voltage hysteresis in **Figure 5c**. These results further testifying metal ions are beneficial for achieving excellent electrochemical kinetic conversion and reducing polarization phenomenon.

Self-discharge performance is an important index to evaluate the LiPSs diffusion during the static time. The cells with different separators were studied by discharging to 1.5 V at a current of 1 C and interrupting for 5 h during each cycle. Apart from that, further interruption for 72 h after the 26th charging was operated. **Figure 5d** shows that the specific capacity drop (Δ) of cells with the modified separators is much smaller than the Celgard assembled cell. And the specific capacity drop rates Δ/Q_{25th} (Q_{25th} is the specific discharge capacity at the 25th cycle) of cells with modified separators (10.4, 7.6, and 7.1% for Por-POP/GN, Por(Mg)-POP/GN and Por(Co)-POP/GN modified separators, respectively) are also much smaller than the cell with the Celgard (24.3%) in **Figure S13**. In addition, the open-circuit voltage (OCV) are 2.27, 2.29, and 2.30 V for Por-POP/GN, Por(Mg)-POP/GN, and Por(Co)-POP/GN modified separators, respectively, whereas for the Celgard, only 2.17 V can be obtained (**Figure 5e**). These results reveal that the modified separator could act as the LiPSs' reservoir and confine the sulfur species loss during a static test, leading to good suppression of the self-discharge behavior.

View Article Online
DOI: 10.1039/D2TA09232H

Journal Name

ARTICLE

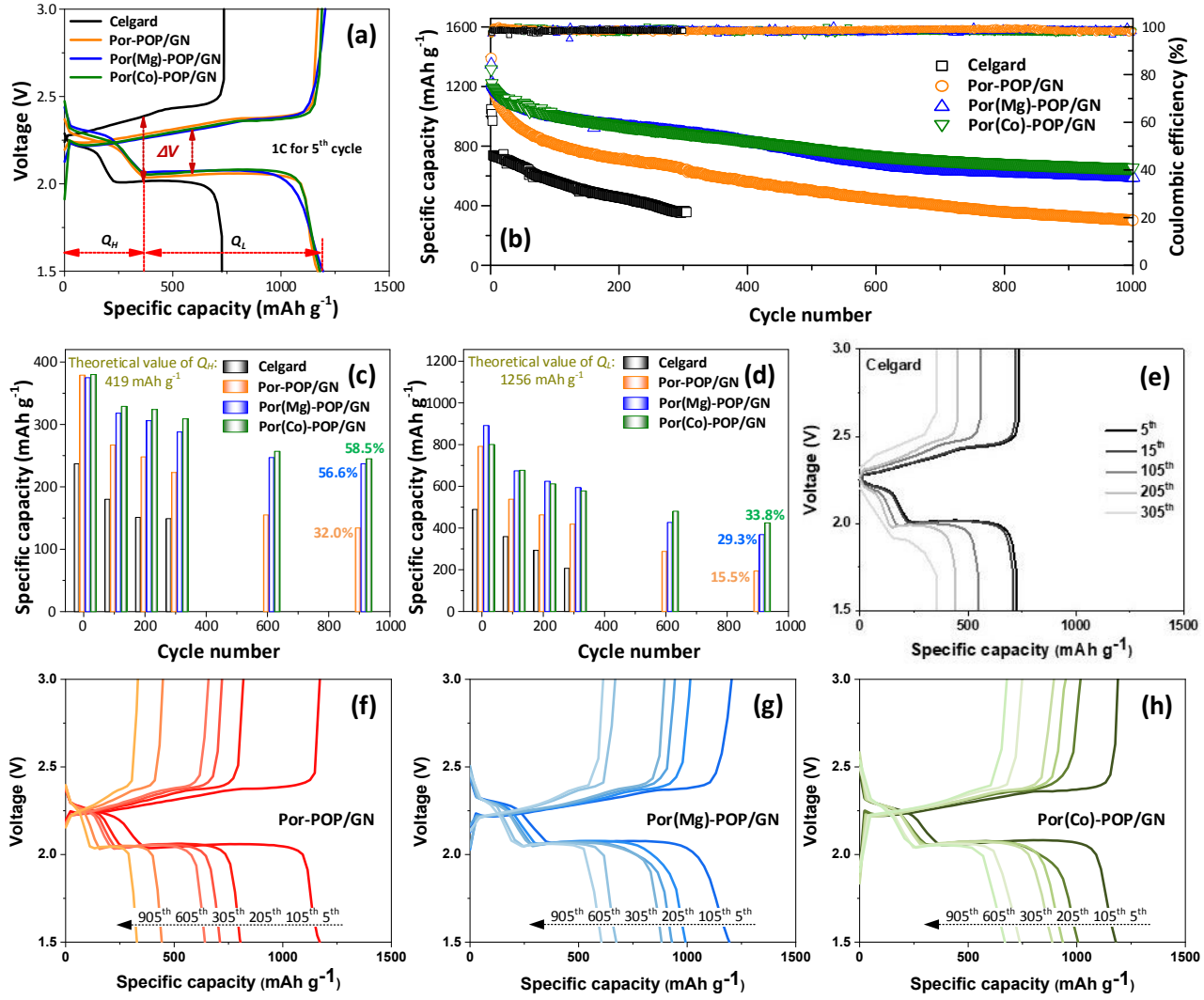

Figure 4. (a) Galvanostatic discharge profiles at 1 C for the 5th cycle; (b) long-term cycling performance of cells with various separators at 1 C, (c) Q_H and (d) Q_L of cells with various separators; charge-discharge curves of cells with (e) the Celgard, (f) Por-POP/GN, (g) Por(Mg)-POP/GN and (h) Por(Co)-POP/GN modified separators at 1 C and 30 °C.

View Article Online
DOI: 10.1039/D2TA09232H

Journal Name

ARTICLE

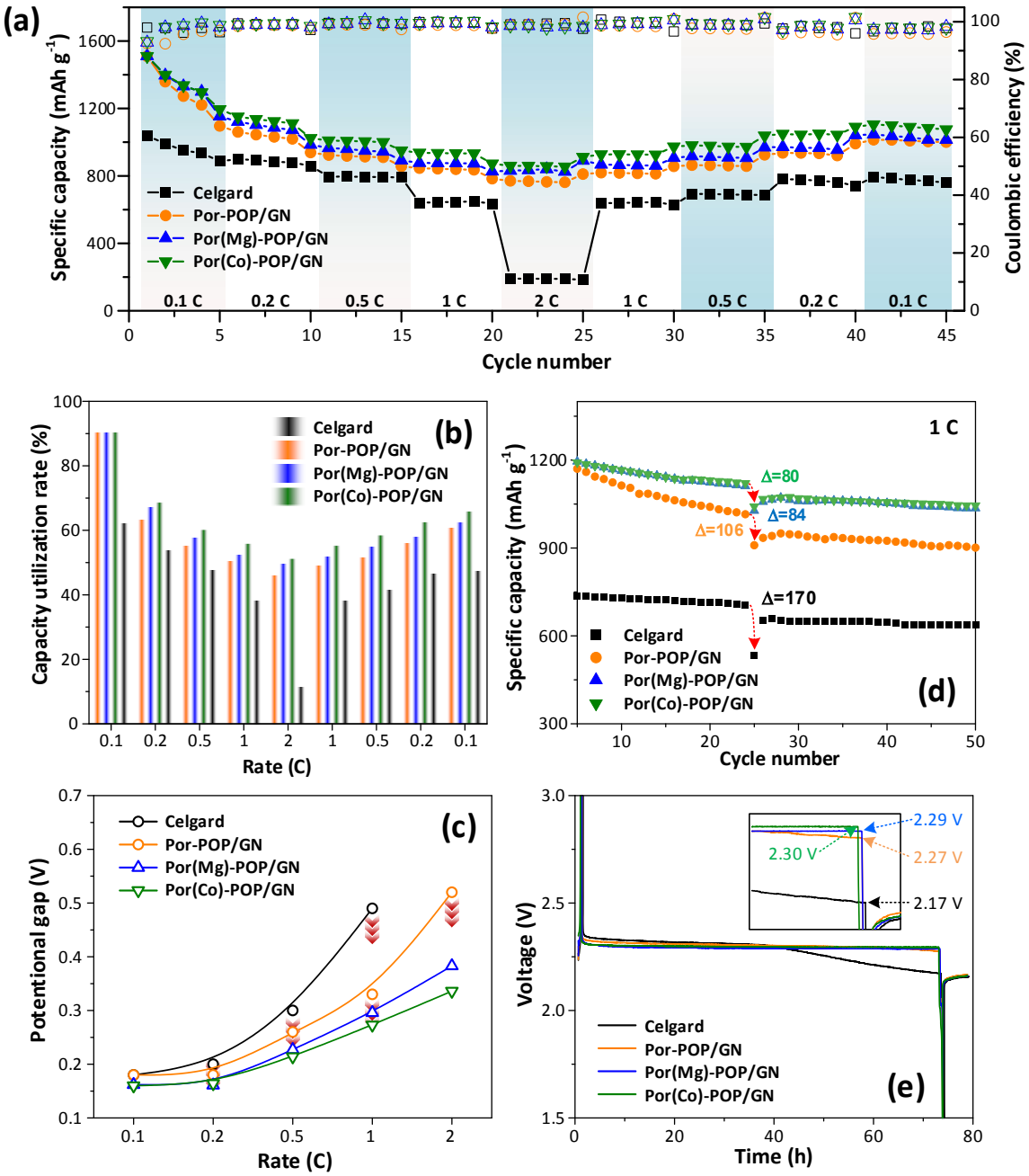

Figure 5. (a) Rate performance, (b) specific capacity utilization rate, and (c) the potential gap of cells with various separators at different rates; (d) the cycling performance and (e) 26th cycled voltage-time profiles of the cells with various separators during the disruption period at 1 C and 30 °C.

High S-loading is a critical design to achieve Li-S batteries with high areal-specific capacity and energy density.[42] Here, the cathode with a higher sulfur loading of 4.0 mg cm^{-2} was applied. As rate performance is shown in Figure 6a, in the first several cycles, the specific capacity gradually increases for the pristine Celgard, demonstrating a slow activation of sulfur due to the sluggish reactions, while without any activation process for the separators manifesting high redox activity. The corresponding

View Article Online
DOI: 10.1039/D2TA09230H

charge-discharge profiles at 0.2, 0.5, and 1 C (Figure S14) also exhibit more stable discharge plateaus and a smaller potential gap for three modified separators than the pristine Celgard. Figure 6b shows the cycling performance at a high current density of 1 C; the cells still can deliver 2.7, 2.8, and 3.1 mAh cm^{-2} for Por-POP/GN, Por(Mg)-POP/GN, and Por(Co)-POP/GN modified separators, respectively, after 100 cycles. Those results demonstrate that functional modifiers possess excellent LiPSs-anchor capability and fast Li^+ diffusion, which is critical in improving the battery performance. Notably, the cells exhibit more apparent enhancement at a high-S loading by introducing catalytic Por(M)-POPs, indicating a more effective conversion of LiPSs in working Li-S batteries. Furthermore, the enhanced sulfur electrochemical redox kinetics is further verified by the galvanostatic intermittent titration technique (GITT) results.[46] Figure S15 shows the GITT curves of cells with modified separators, where the dash lines indicate the state of electrochemical equilibrium during multiple resting periods.[47] After coating the functional modifier on the Celgard, the ΔV became smaller between operation and equilibrium during the repeated charge-discharge processes, which is displayed in the *IR* drop variation in Figure 6c, further confirming much-alleviated polarization and improved electrochemical kinetics. The EIS analysis of high S-loading cells was furtherly carried out to monitor the resulting cells' inner resistance before and after cycling. Before cycling in Figure 6d, the Nyquist plots mainly consist of a depressed semicircle representing the charge transfer resistance (R_{ct}) across interfaces. After cycling to stable, one extra semicircle appeared for all cycled cells, which can be attributed to the migration of Li^+ through the passivation film.[48] The corresponding equivalent circuit models are presented in the inset. The relatively lower R_{ct} of modified separators than the Celgard indicates better cross-interface transport performance and somewhat thinner passivation layers on both cathode and anode surfaces.[11] Those improved electrochemical performances are supposed to enhance the battery's cycle stability and rate capacity even at a high S-loading.

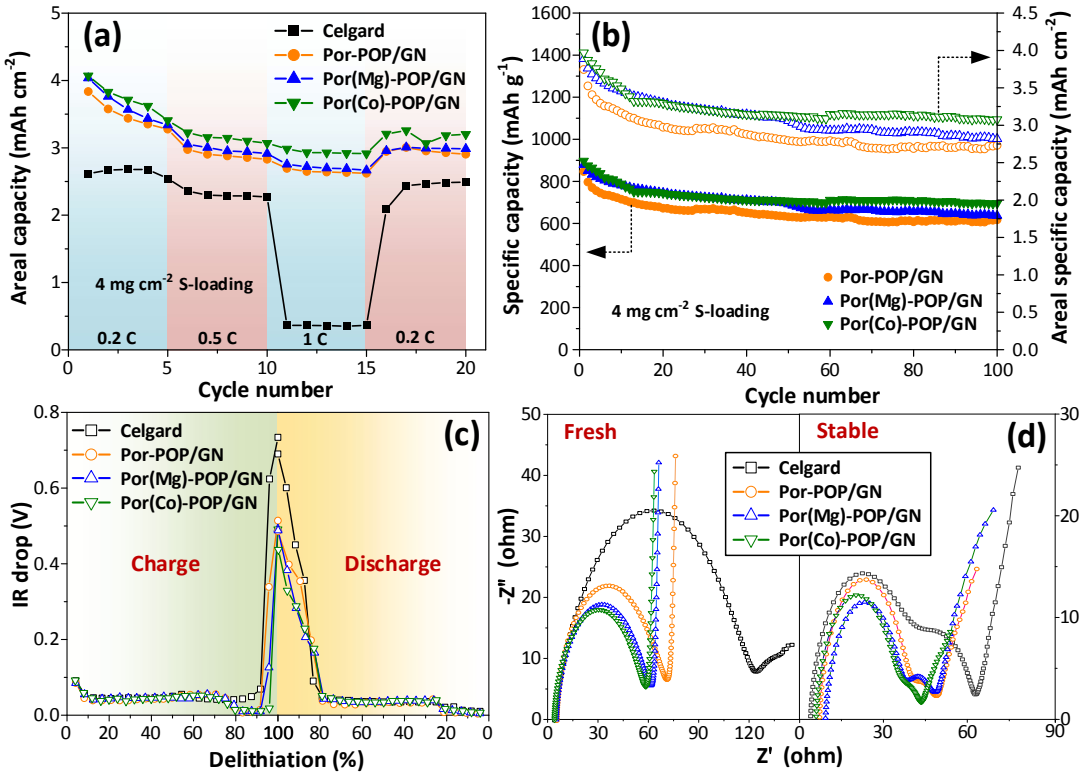

Figure 6. (a) rate performance of high S-loading cells with different separators under the rate of 0.2, 0.5, and 1 C; (b) cycle performance of high S-loading cells with various separators at 1 C; (c) IR drops during the charge-discharge process of the high S-loading cells with different separators; (d) ESI of the high S-loading cells with different separators before and after cycling.

To better intuitively observe Li deposition, SEM and EDS mapping of the Li anode surface from the cycled cells are displayed in Figure 7a-7d**.** The surface morphology of the Li anode for cycled Celgard reveals bulky rough dendrites owing to the unwanted reaction between the dissolved LiPSs and Li anode during cycling. At the same time, the cycled Por-POP/GN modified separator shows particle-like microstructure, and the cycled Por(M)-POP/GN modified separators exhibit smooth plane microstructure. Those results demonstrate that the introduced modifiers could effectively retard the formation and growth of Li dendrite, especially for the catalytic modifiers, attributing to the improved electrochemical kinetic, which could increase sulfur species conversion instead of shutting to Li anode. Furthermore, the S-cathodes of cycled cells were immersed in tetrahydrofuran (THF). As shown in Figure S16, the color change in the resulting THF solution and corresponding

View Article Online
DOI: 10.1039/D3TA00373H

UV-vis spectra further verified the synergistic effect for trapping and catalyzing LiPSs by the Por(M)-POP/GN modifiers during long-term charge and discharge processes. The chemical interaction between the LiPS and Por(M)-POP/GN was further investigated by the DFT calculations (**Figure 7e**). In the case of Por(Co)-POP, it can be seen that both the porphyrin molecule and imidazolium connector exhibited higher binding energies to soluble LiPSs ($Li_2S_{4,6,8}$) than the case of GN, indicating the enhanced confinement of LiPS by Por(M)-POP modifiers (**Figure 7e**).

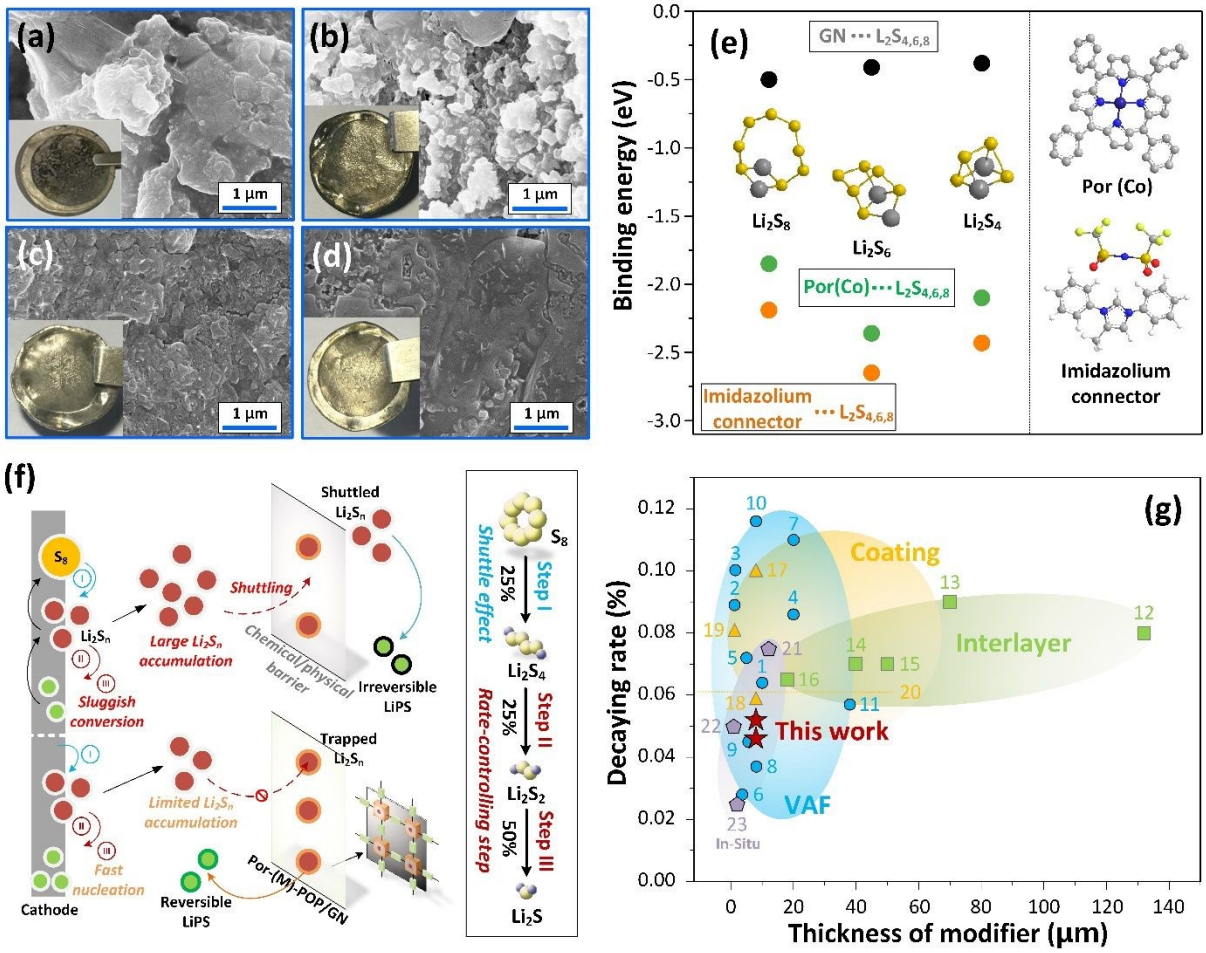

Figure 7. Digital and SEM images of Li metal from disassembled cells with (a) the Celgard, (b) Por-POP/GN, (c) Por(Mg)-POP/GN, and (d) Por(Co)-POP/GN modified separators after cycling; (e) binding energies between the $Li_2S_{4,6,8}$ on the surface of Por(Co)-POP in the electrochemical process; (f) the influence of the LiPS for the typically modified separator with chemical/physical barriers and Por(M)-POP/GN modified separators in the electrochemical process; (g) performance of Li-S batteries with multi-functional modifiers and pure S cathode in this study and previously reported studies for the past five years (1: MoS_2@CF-NRGO; 2: Li-MOF/RGO; 3: MOF/RGO; 4: Nb_2O_5/RGO; 5: HVS; 6: LNS/CB; 7: CNF; 8: VOH@PANI/CNT; 9: $WN_{0.67}$@NG; 10: rGO@MoS_2; 11: $NiCo_2O_4$; 12: CoFe@CNFs; 13: LMO/SP/NF; 14: CNT@C; 15: Pd_3Co/MWCNT; 16: Al_2O_3/C@OSi; 17: ZNS-RGA; 18: CoFe@NC; 19: SVO/AB; 20: Ni@C/G; 21: $CoSO_4$; 22: TpPa-SO_3H; 23: SNFs/PDA; detail as shown in SI).

As shown in **Figure 7f**, the introduced Por(M)-POP modifier simultaneously provides the chemical anchor and physical confinement to trap the dissolved Li_2S_n, avoiding the shuttled LiPSs to further reduce to solid Li_2S_2/Li_2S as irreversible active sulfur in the following cycling processes. And the active Por(M) is proposed as an effective catalysis for accelerating the deposition of Li_2S_n into insoluble Li_2S_2/Li_2S and decelerating the accumulation of soluble LiPS, leading to a limited LiPS shuttling that is not trapped in time. To demonstrate an improvement of the cell with our modified separators, the fabrication strategy, modifier thickness, and the cell decaying were evaluated with previously reported studies. The modified separators prepared by a promising approach in practical production have a thinner modifier thickness but yield a lower decaying rate for the cell, which can be regarded as promising separators to meet the requirements of high energy density and long cycling stability in Li-S batteries. As shown in **Figure 7g** and **Table S4**, the modified separators prepared by the vacuum assistant filtration (VAF) and in-situ growth strategies yield a wide range of decaying rates at thicknesses of 0.9~38 μm. Interestingly, thinner thicknesses of <2 μm are found in some modified separators prepared by VAF and in-situ growth compared to blade-coating and interlayer strategies, indicating a higher energy density can be reached by employing these separators. However, limited materials size, dimensional restrictions, and fabrication time for both approaches limit their applicability to some extent. Inserting an interlayer seems to be a potential solution to address these problems, but a thick modified layer (18~132 μm)

is required to obtain a free-standing layer for the battery assembly. Blade-coating is the most promising approach in practical production owing to its easy operation with no specific equipment requirements and large-scale production potential. Our modified separators are fabricated by a simple and cost-effective blade-coating approach and show low decaying rates of 0.052 and 0.046 % under a thin modifier layer. Besides, to put our work in perspective with respect to published studies of Li-S cells enhanced by introducing single-atom catalyst function (**Table S4**), our Por(M)-POP/GN modified separators clearly reveal a significant improvement in electrochemical performances, thus opening up a route to a new separator engineering for fabricating multi-functional separator for Li-S batteries.

Conclusions

In summary, we have successfully designed electrolyte and Li-ions accessible, an electrochemical catalytic function integrated modifier of Por(M)-POP to improve the LiPS adsorption and accelerate the redox reaction kinetics for high-performance Li-S batteries. With the lithiophilic imidazolium connector, more functional groups in Por(M)-POP are inclined to facilitate electrolyte infiltration and Li-ion transport as well as interact with LiPSs for high Li-ion diffusion but low LiPS shutting. In addition, the electrochemically catalytic Por(M) within the porous PIL framework combined with electrically conductive GN effectively shortens the electron transfer route and promotes electrocatalytic activity for Li-S batteries. The LiPS redox kinetic is significantly improved due to the high Li-ion diffusion, electro-conduction, and effective LiPS adsorption. Benefiting from these synergistic effects, the Por(M)-POP/GN modified separator effectively suppresses LiPSs shuttling and promotes the kinetics of the multiphase sulfur redox reactions; therefore, the resultant cells display high sulfur utilization, robust cycling life, good rate performance, low self-discharge behavior, and negligible Li dendrite. Finally, as a POP with catalytic and ion conductive sites in the skeleton, we envision that the proof-of-principle research may provide an opportunity to explore the structure-property relationship between the functional modifier and cell performance. We are now working on designing and synthesizing other multi-functional POPs, not only addressing the problem of severe shuttling and very sluggish conversion for LiPSs but also with low-cost and large scalable separators in Li-metal batteries.

Acknowledgements

We acknowledge analytical and testing assistance from the Instrumentation Center at NSYSU.

Conflicts of interest

The authors declare no conflict of interest.

Notes and references

View Article Online
DOI: 10.1039/D2TA09232H

(1) Feng, S.; Zhong, H.; Song, J. H.; Zhu, C. Z.; Dong, P. P.; Shi, Q. R.; Liu, D.; Li, J. C.; Chang, Y. C.; Beckman, S. P.et al. Catalytic Activity of Co-X (X = S, P, O) and Its Dependency on Nanostructure/Chemical Composition in Lithium-Sulfur Batteries. *Acs Applied Energy Materials* **2018,** *1* (12), 7014.

(2) Yang, W.; Yang, W.; Song, A. L.; Sun, G.; Shao, G. J. 3D interconnected porous carbon nanosheets/carbon nanotubes as a polysulfide reservoir for high performance lithium-sulfur batteries. *Nanoscale* **2018,** *10* (2), 816.

(3) Zhang, L.; Wan, F.; Wang, X.; Cao, H.; Dai, X.; Niu, Z.; Wang, Y.; Chen, J. Dual-Functional Graphene Carbon as Polysulfide Trapper for High-Performance Lithium Sulfur Batteries. *ACS applied materials & interfaces* **2018,** *10* (6), 5594.

(4) Jia-Qi Huang, § Ting-Zhou Zhuang,†,§ Qiang Zhang,*,† Hong-Jie Peng,† Cheng-Meng Chen,‡ and Fei Wei†. Permselective Graphene Oxide Membrane for Highly Stable and Anti-Self-Discharge Lithium-Sulfur Batteries. *ACS nano* **2015,** *9* (3), 3002.

(5) Babu, G.; Masurkar, N.; Al Salem, H.; Arave, L. M. R. Transition Metal Dichalcogenide Atomic Layers for Lithium Polysulfides Electrocatalysis. *Journal of the American Chemical Society* **2017,** *139* (1), 171.

(6) Shi, Q. X.; Pei, H. J.; You, N.; Wu, J.; Xiang, X.; Xia, Q.; Xie, X. L.; Jin, S. B.; Ye, Y. S. Large-scaled covalent triazine framework modified separator as efficient inhibit polysulfide shuttling in Li-S batteries. *Chem. Eng. J.* **2019,** *375*, 121977.

(7) Yuan, H.; Peng, H. J.; Li, B. Q.; Xie, J.; Kong, L.; Zhao, M.; Chen, X.; Huang, J. Q.; Zhang, Q. Conductive and Catalytic Triple-Phase Interfaces Enabling Uniform Nucleation in High-Rate Lithium-Sulfur Batteries. *Adv. Energy Mater.* **2019,** *9* (1), 8.

(8) Lin, H. B.; Zhang, S. L.; Zhang, T. R.; Ye, H. L.; Yao, Q. F.; Zheng, G. W.; Lee, J. Y. Simultaneous Cobalt and Phosphorous Doping of MoS_2 for Improved Catalytic Performance on Polysulfide Conversion in Lithium-Sulfur Batteries. *Adv. Energy Mater.* **2019,** *9* (38), 9.

(9) Abbas, S. A.; Ding, J.; Wu, S. H.; Fang, J.; Boopathi, K. M.; Mohapatra, A.; Lee, L. W.; Wang, P. C.; Chang, C. C.; Chu, C. W. Modified Separator Performing Dual Physical/Chemical Roles to Inhibit Polysulfide Shuttle Resulting in Ultrastable Li-S Batteries. *ACS nano* **2017,** *11* (12), 12436.

(10) Gou, J.; Zhang, H.; Yang, X.; Chen, Y.; Yu, Y.; Li, X.; Zhang, H. Quasi-Stable Electroless Ni-P Deposition: A Pivotal Strategy to Create Flexible Li-S Pouch Batteries with Bench Mark Cycle Stability and Specific Capacity. *Advanced Functional Materials* **2018**, 28 (20), 1707272.

(11) Zhai, P. Y.; Peng, H. J.; Cheng, X. B.; Zhu, L.; Huang, J. Q.; Zhu, W. C.; Zhang, Q. Scaled-up fabrication of porous-graphene-modified separators for high-capacity lithium-sulfur batteries. *Energy Storage Materials* **2017,** *7*, 56.

(12) Zhang, L.; Chen, X.; Wan, F.; Niu, Z.; Wang, Y.; Zhang, Q.; Chen, J. Enhanced Electrochemical Kinetics and Polysulfide Traps of Indium Nitride for Highly Stable Lithium-Sulfur Batteries. *ACS Nano* **2018,** *12* (9), 9578.

(13) Zhang, L.; Liu, D.; Muhammad, Z.; Wan, F.; Xie, W.; Wang, Y.; Song, L.; Niu, Z.; Chen, J. Single Nickel Atoms on Nitrogen-Doped Graphene Enabling Enhanced Kinetics of

Lithium-Sulfur Batteries. *Adv Mater* **2019,** *31* (40), 1903955.

(14) Chen, K.; Zhang, G.; Xiao, L.; Li, P.; Li, W.; Xu, Q.; Xu, J. Polyaniline Encapsulated Amorphous V_2O_5 Nanowire-Modified Multi-Functional Separators for Lithium-Sulfur Batteries. *Small Methods* **2021,** *5* (3), 2001056.

(15) Song, Z.; Zhang, L.; Doyle-Davis, K.; Fu, X.; Luo, J.L.; Sun, X. Recent Advances in MOF-Derived Single Atom Catalysts for Electrochemical Applications. *Advanced Energy Materials* **2020,** *10* (38), 2001561.

(16) Xie, J.; Li, B.Q.; Peng, H.J.; Song, Y.W.; Zhao, M.; Chen, X.; Zhang, Q.; Huang, J.Q. Implanting Atomic Cobalt within Mesoporous Carbon toward Highly Stable Lithium-Sulfur Batteries. *Adv Mater* **2019,** *31* (43), 1903813.

(17) Zhou, G.; Zhao, S.; Wang, T.; Yang, S.Z.; Johannessen, B.; Chen, H.; Liu, C.; Ye, Y.; Wu, Y.; Peng, Y.et al. Theoretical Calculation Guided Design of Single-Atom Catalysts toward Fast Kinetic and Long-Life Li-S Batteries. *Nano Lett* **2020,** *20* (2), 1252.

(18) Gao, W.-Y.; Chrzanowski, M.; Ma, S. Metal-metalloporphyrin frameworks: a resurging class of functional materials. *Chem Soc Rev* **2014,** *43* (16), 5841.

(19) Senge, M. O.; Sergeeva, N. N.; Hale, K. J. Classic highlights in porphyrin and porphyrinoid total synthesis and biosynthesis. *Chem Soc Rev* **2021,** *50* (7), 4730.

(20) Zhao, C.X.; Li, X.Y.; Zhao, M.; Chen, Z.X.; Song, Y.W.; Chen, W.J.; Liu, J.N.; Wang, B.; Zhang, X.Q.; Chen, C.M.et al. Semi-Immobilized Molecular Electrocatalysts for High-Performance Lithium-Sulfur Batteries. *J Am Chem Soc* **2021,** *143* (47), 19865.

(21) Jeong, K.; Kim, J.M.; Kim, S. H.; Jung, G. Y.; Yoo, J.; Kim, S.H.; Kwak, S. K.; Lee, S.Y. Carbon-Nanotube-Cored Cobalt Porphyrin as a 1D Nanohybrid Strategy for High-Performance Lithium-Ion Battery Anodes. *Adv Funct Mater* **2019,** *29* (24), 1806937.

(22) Kong, L.; Li, B.Q.; Peng, H.J.; Zhang, R.; Xie, J.; Huang, J.Q.; Zhang, Q. Porphyrin-Derived Graphene-Based Nanosheets Enabling Strong Polysulfide Chemisorption and Rapid Kinetics in Lithium-Sulfur Batteries. *Advanced Energy Materials* **2018,** *8* (20), 1800849.

(23) Hu, S.; Yi, M.; Huang, X.; Wu, D.; Lu, B.; Wang, T.; Li, N.; Zhu, Z.; Liu, X.; Zhang, J. Cobalt-doped porphyrin-based porous organic polymer-modified separator for high-performance lithium–sulfur batteries. *J Mater Chem A* **2021,** *9* (5), 2792.

(24) Li, B.Q.; Zhang, S.Y.; Kong, L.; Peng, H.J.; Zhang, Q. Porphyrin Organic Framework Hollow Spheres and Their Applications in Lithium-Sulfur Batteries. *Adv Mater* **2018,** *30* (23), 1707483.

(25) Liao, H.; Wang, H.; Ding, H.; Meng, X.; Xu, H.; Wang, B.; Ai, X.; Wang, C. A 2D porous porphyrin-based covalent organic framework for sulfur storage in lithium-sulfur batteries. *J Mater Chem A* **2016,** *4* (19), 7416.

(26) Ebrahimi, A.; Krivosudský, L. Metalloporphyrin Metal–Organic Frameworks: Eminent Synthetic Strategies and Recent Practical Exploitations. *Molecules* **2022,** *27* (15), 4917.

(27) Ye, Y.S.; Wang, H.; Bi, S.G.; Xue, Y.; Xue, Z.G.; Zhou, X.P.; Xie, X.L.; Mai, Y.W. High performance composite polymer electrolytes using polymeric ionic liquid-functionalized graphene molecular brushes. *J Mater Chem A* **2015,** *3* (35), 18064.

(28) Gao, X.; DelaCruz, S.; Zhu, C. H.; Cheng, S. Y.; Gardner, D.; Xie, Y. H.; Carraro, C.; Maboudian, R. Surface functionalization of carbon cloth with cobalt-porphyrin-based metal organic framework for enhanced electrochemical sensing. *Carbon* **2019,** *148*, 64.

(29) Dubecky, F.; Kindl, D.; Hubik, P.; Micusik, M.; Dubecky, M.; Bohacek, P.; Vanko, G.; Gombia, E.; Necas, V.; Mudron, J. A comparative study of Mg and Pt contacts on semi-insulating GaAs: Electrical and XPS characterization. *Appl. Surf. Sci.* **2017,** *395*, 131.

(30) Andreeva, N. P.; Larionov, A. V.; Grafov, O. Y.; Golubchikov, O. A.; Kazanskii, L. P.; Kuznetsov, Y. I. The Adsorption of 5,10,15,20-Tetrakis(N-methylpyridyl-4')porphine Tetratosylate on the Surface of Nickel from an Aqueous Solution. *Prot. Met. Phys. Chem. Surf.* **2018,** *54* (7), 1276.

(31) Zhu, K.; Luo, Q.; Kang, S. Z.; Qin, L. X.; Li, G. D.; Li, X. Q. The study of a novel cobalt-implanted pyridylporphyrin/graphene oxide nanohybrid for enhanced photocatalytic hydrogen evolution and its electron transfer mechanism. *Nanoscale* **2018,** *10* (39), 18635.

(32) Chen, J.; Zhong, M. M.; Tao, L.; Liu, L. N.; Jayakumar, S.; Li, C. Z.; Li, H.; Yang, Q. H. The cooperation of porphyrin-based porous polymer and thermal-responsive ionic liquid for efficient CO_2 cycloaddition reaction. *Green Chemistry* **2018,** *20* (4), 903.

(33) Zhang, L. S.; Jie, S. S.; Liu, Z. G. Bicontinuous mesoporous Co, N co-doped carbon catalysts with high catalytic performance for ethylbenzene oxidation. *New J. Chem.* **2019,** *43* (19), 7275.

(34) Lindsey, J. S.; Ptaszek, M.; Taniguchi, M. Simple Formation of an Abiotic Porphyrinogen in Aqueous Solution. *Orig. Life Evol. Biosph.* **2009,** *39* (6), 495.

(35) Xiao, Z.; Li, L.; Tang, Y.; Cheng, Z.; Pan, H.; Tian, D.; Wang, R. Covalent organic frameworks with lithiophilic and sulfiphilic dual linkages for cooperative affinity to polysulfides in lithium-sulfur batteries. *Energy Storage Materials* **2018,** *12*, 252.

(36) Sun, W.; Sun, X.; Peng, Q.; Wang, H.; Ge, Y.; Akhtar, N.; Huang, Y.; Wang, K. Nano-MgO/AB decorated separator to suppress shuttle effect of lithium-sulfur battery. *Nanoscale Advances* **2019,** *1* (4), 1589.

(37) Hu, Q.; Lu, J.; Yang, C.; Zhang, C.; Hu, J.; Chang, S.; Dong, H.; Wu, C.; Hong, Y.; Zhang, L. Promoting Reversible Redox Kinetics by Separator Architectures Based on CoS_2/HPGC Interlayer as Efficient Polysulfide-Trapping Shield for Li–S Batteries. *Small* **2020,** *16* (34), 2002046.

(38) Wang, Z.; Wang, B.; Yang, Y.; Cui, Y.; Wang, Z.; Chen, B.; Qian, G. Mixed-Metal-Organic Framework with Effective Lewis Acidic Sites for Sulfur Confinement in High-Performance Lithium-Sulfur Batteries. *ACS applied materials & interfaces* **2015,** *7* (37), 20999.

(39) Yuan, Z.; Peng, H. J.; Hou, T. Z.; Huang, J. Q.; Chen, C. M.; Wang, D. W.; Cheng, X. B.; Wei, F.; Zhang, Q. Powering Lithium-Sulfur Battery Performance by Propelling Polysulfide Redox at Sulfiphilic Hosts. *Nano letters* **2016,** *16* (1), 519.

(40) Huang, X.; Tang, J. Y.; Luo, B.; Knibbe, R.; Lin, T. G.; Hu, H.; Rana, M.; Hu, Y. X.; Zhu, X. B.; Gu, Q. F.et al. Sandwich-Like Ultrathin TiS_2 Nanosheets Confined within N, S Codoped Porous Carbon as an Effective Polysulfide Promoter in

View Article Online
DOI: 10.1039/D2TA09232H

Lithium-Sulfur Batteries. *Adv. Energy Mater.* **2019,** *9* (32), 9.

(41) Pu, J.; Shen, Z.; Zheng, J.; Wu, W.; Zhu, C.; Zhou, Q.; Zhang, H.; Pan, F. Multifunctional Co_3S_4@sulfur nanotubes for enhanced lithium-sulfur battery performance. *Nano Energy* **2017,** *37*, 7.

(42) Xiang, X.; Wu, J. Y.; Shi, Q. X.; Xia, Q.; Xue, Z. G.; Xie, X. L.; Ye, Y. S. Mesoporous silica nanoplates facilitating fast Li+ diffusion as effective polysulfide-trapping materials for lithium-sulfur batteries. *J Mater Chem A* **2019,** *7* (15), 9110.

(43) Yang, X. F.; Gao, X. J.; Sun, Q.; Jand, S. P.; Yu, Y.; Zhao, Y.; Li, X.; Adair, K.; Kuo, L. Y.; Rohrer, J.et al. Promoting the Transformation of Li_2S_2 to Li_2S: Significantly Increasing Utilization of Active Materials for High-Sulfur-Loading Li-S Batteries. *Adv. Mater.* **2019,** *31* (25), 10.

(44) Lin, H. B.; Zhang, S. L.; Zhang, T. R.; Cao, S.; Ye, H. L.; Yao, Q. F.; Zheng, G. W.; Lee, J. Y. A Cathode-Integrated Sulfur-Deficient Co_9S_8 Catalytic Interlayer for the Reutilization of "Lost" Polysulfides in Lithium-Sulfur Batteries. *ACS nano* **2019,** *13* (6), 7073.

(45) Zahid Ali Ghazi, X. H., Abdul Muqsit Khattak, Niaz Ali Khan, Bin Liang, Azhar Iqbal,Jinxin Wang, Haksong Sin, Lianshan Li,* and Zhiyong Tang*. MoS_2-Celgard Separator as Efficient Polysulfide Barrier for Long-Life Lithium–Sulfur Batteries. *Adv. Mater.* **2017,** *29*, 1606817.

(46) Luo, L.; Chung, S.H.; Manthiram, A. A three-dimensional self-assembled SnS_2-nano-dots@graphene hybrid aerogel as an efficient polysulfide reservoir for high-performance lithium–sulfur batteries. *Journal of Materials Chemistry A* **2018,** *6* (17), 7659.

(47) Li, G.; Lei, W.; Luo, D.; Deng, Y.P.; Wang, D.; Chen, Z. 3D Porous Carbon Sheets with Multidirectional Ion Pathways for Fast and Durable Lithium-Sulfur Batteries. *Adv. Energy Mater.* **2018,** *8* (8), 1702381.

(48) Jiang, Y.; Chen, F.; Gao, Y.; Wang, Y. Y.; Wang, S. S.; Gao, Q.; Jiao, Z.; Zhao, B.; Chen, Z. W. Inhibiting the shuttle effect of Li-S battery with a graphene oxide coating separator: Performance improvement and mechanism study. *Journal of Power Sources* **2017,** *342*, 929.